Requirements for the containment of COVID-19 disease outbreaks through periodic testing, isolation, and quarantine

Shannon R. Serrao[1], Shengfeng Deng[1,2], Priyanka[1], Ruslan I. Mukhamadiarov[1], Lauren M. Childs[3], Uwe C. Täuber[1,4]

[1]Department of Physics and Center for Soft Matter and Biological Physics, Virginia Tech, Blacksburg, VA 24061, USA
[2]Key Laboratory of Quark and Lepton Physics (MOE) and Institute of Particle Physics, Central China Normal University, Wuhan 430079, China
[3]Department of Mathematics, Virginia Tech, Blacksburg, VA 24061, USA
[4]Faculty of Health Sciences, Virginia Tech, Blacksburg, VA 24061, USA

Abstract

We employ individual-based Monte Carlo computer simulations of a stochastic SEIR model variant on a two-dimensional Newman–Watts small-world network to investigate the control of epidemic outbreaks through periodic testing and isolation of infectious individuals, and subsequent quarantine of their immediate contacts. Using disease parameters informed by the COVID-19 pandemic, we investigate the effects of various crucial mitigation features on the epidemic spreading: fraction of the infectious population that is identifiable through the tests; testing frequency; time delay between testing and isolation of positively tested individuals; and the further time delay until quarantining their contacts as well as the quarantine duration. We thus determine the required ranges for these intervention parameters to yield effective control of the disease through both considerable delaying the epidemic peak and massively reducing the total number of sustained infections.

1 Introduction

In December 2019, a novel coronavirus, known as SARS-CoV-2, emerged in the human population and has caused an on-going, widespread pandemic. COVID-19, the disease caused by SARS-CoV-2 has resulted in significant losses in lives, health, and the economy. With more than 30 million cases and 1 million deaths, at the time of writing, additional methods are needed to accurately understand and predict the spread of the disease. Mathematical models are important tools to quantify the non-linear interactions inherent to infectious disease spread [1, 2].

The dynamics of an incubation-type disease in a population can be mathematically captured by variants of the Susceptible-Exposed-Infected-Recovered (*SEIR*) model [3, 4, 5]. In the SEIR compartmental model, individuals may assume four distinct states: *S - Susceptible, E - Exposed, I - Infected,* and *R - Recovered*. Mean-field rate equations are often utilized to encode the SEIR reactions and predict how the total number of individuals in each state evolves with time. However, these coupled ordinary differential equations invoke a mass-action like factorization of higher moments into powers of compartmental population numbers, and hence neglect temporal fluctuations and/or spatial variations. Specifically, the rate equation description cannot properly account for the strong number fluctuations that drive the continuous phase transition when the system is near the epidemic threshold, nor for spatially correlated clusters and spreading fronts that are induced by the disease's propagation through nearest-contact infection [6, 7]. Consequently, the rate equation approximation cannot capture stochastic extinction events if the disease parameters are set below or near the epidemic threshold, and also severely underestimates the ultimate prevalence of the above-threshold epidemic in the population [8, 9].

In modern human societies, disease spreading in a confined spatial environment is most adequately described by a graph model that represents social contact interactions, and that allows for both short-range diffusive propagation as well as farther-reaching contacts along travel routes. While direct links on a lattice would enable the infection to spread from the carriers to their immediate susceptible neighbors, additional long-range connections emulate 'express' routes for disease transmission to spatially distant regions. For example, a detailed study of close proximity interactions in an American high school examined more than 700,000 interactions and found a network with small-world properties [10]. Realistic contact networks are rather com-

plex, and in fact tend to vary from one local community to another [11]. Therefore, it is more convenient and parsimonious to work with a generic network model that is not constrained by the availability of the real-network data.

The unusual abundance of non-symptomatic infected individuals constitutes a major obstacle in containing the spread of SARS-CoV-2 [12, 13]. Such asymptomatic or pre-symptomatic individuals do not realize they are infected or transmitting and thus go about their typical daily routine, leading to additional spread of the virus. Furthermore, a scant availability of tests, delays in the process, and potential reluctance of undergoing testing and isolation procedures, may substantially undermine mitigation efforts. In practice, and especially for a highly contagious disease such as COVID-19 with a sizeable fraction of non-symptomatic infections, even with a repeated and effective testing regimen it is impossible to capture and isolate every single infected individual. To deal with a significant fraction of unidentified infectious individuals, it is necessary to capture the direct neighborhood of confirmed disease carriers, and quarantine these individuals. That is, even if a person who had direct contact with the identified infected individual does not show any symptoms of infection, that person should still be separated from the general population. Only then can further infection propagation through unidentified (perhaps asymptomatic) disease carriers be controlled effectively.

Our goal here is to investigate how a properly implemented periodic testing and isolation regimen combined with quarantining infectious individuals' contacts may quell the disease spread. While this central idea of repeatedly screening the population, isolating positively tested individuals, and quarantining their immediate contacts, irrespective of their infection status, is straightforward and long-established, its efficacy depends crucially on the ability to determine who is infectious in a timely manner [14, 15, 16]. For the current epidemic, delays occur due to the the period before receiving test results, as well as the (unavoidable) time lapse between the identification of infectious individuals and their placement in isolation, and the subsequent time until all infectious persons' contacts are quarantined. To properly incorporate these delays, and their impact on disease transmission in a heterogeneous network, we need to consider a fully stochastic and properly spatially extended representation of the SEIR model.

We find that the fraction of identified infectious individuals and the testing period both play decisive roles in containing the infection outbreak; in

contrast, within reasonable bounds, the delays in testing and quarantining, as well as the quarantine duration, all affect the course of the outbreak and its extent in a much more limited manner. In prioritizing resources to achieve an optimized testing / isolation / quarantine strategy, primary emphasis should be placed on frequent and comprehensive testing, less on reducing minor delays in reporting test results and effective contact tracing.

2 Model description

2.1 Modified stochastic SEIR model on a two-dimensional Newman–Watts small-world network

In this model, the disease spread is represented by three characteristic reactions that we consider as independent stochastic processes: $S + I \to E + I$ with the reaction rate r, $E \to I$ with the reaction rate b (related to the inverse incubation period), $I \to R$ with reaction rate a (given by the inverse recovery period). The basic reproduction number for the system is proportional to the ratio of the infection to the recovery reaction rates $\mathcal{R}_0 \propto r/a$, with a proportionality constant that is given by the mean number of contacts of each individual [17]. To capture potential limitations for effective testing and isolation protocols in our mathematical model, we replace the infectious state in the SEIR model with two distinct configurations that we term *identified infectious* (I) and *unidentified infectious* (A) states, respectively. Here, "identification" is to be understood as an umbrella term that encapsulates the overall capability of the testing procedure to identify and subsequently isolate infected individuals. That is, if the entire population is tested, then only the fraction of identified infectious individuals will be detected and quarantined, i.e., temporarily removed from the system, which has the effect of disrupting their future infection chain with other susceptible individuals. However, any unidentified infectious individuals will continue to spread the disease until they ultimately recover from it. The schematics of this modified SEIR model variant is displayed in Fig. 1a. The reactions $E \to I$ and $E \to A$ may occur with the respective rates IID b and (1−IID) b, where IID denotes the fraction of identified infectious individuals, an important independent parameter in our study. Note that we assume identical infection and recovery rates for individuals in both the identified or unidentified states.

In this paper, we utilize a Newman–Watts small-world network [18] in two

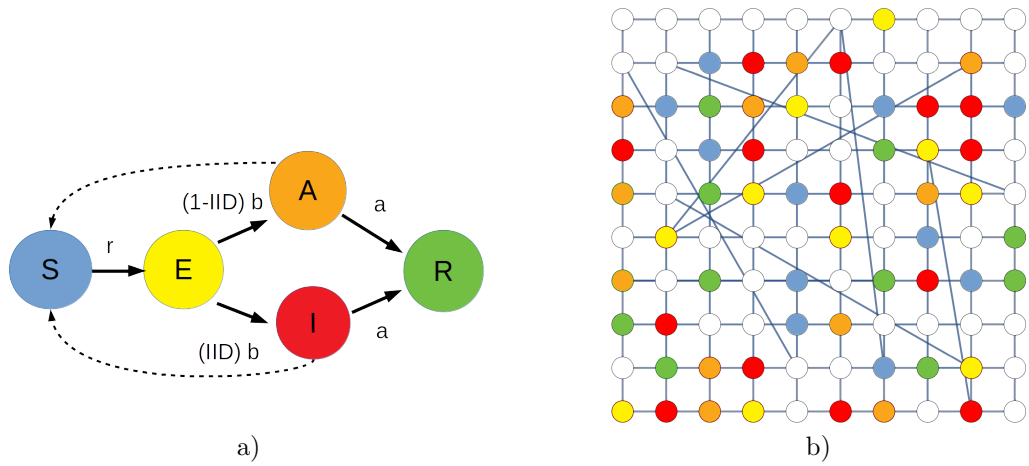

Figure 1: (a) Flow diagram for the modified SEIR model. The arrows between different states represent the stochastic reactions with the appropriate reaction rates. Our modification entails replacing the infectious state with distinct *identified infectious* and *unidentified infectious* states. The fraction IID of identified infectious individuals constitutes a crucial adjustable parameter in the model. (b) Schematic construction of a Newman–Watts small-world network in two spatial dimensions. It is obtained from a regular square lattice (with periodic boundary conditions, i.e., on a torus) through adding long-distance connections between randomly selected lattice sites. The graph displays a modified SEIR model configuration snapshot with sites residing in empty (white), susceptible (blue), exposed/incubative (yellow), identified infectious (red), unidentified infectious (orange), or recovered (green) states (color coding as in a).

dimensions as a suitable spatial framework for our individual-based Monte Carlo simulations of the COVID-19 epidemic propagation [9]. The two-dimensional Newman–Watts small-world network consists of a regular square lattice with L sites in each direction, and additional long-distance links, c.f. Fig. 1b. Thus, it comprises $2L\,(L-1)$ short-range links that connect the nearest-neighbor lattice vertices, and $2\phi L^2$ additional long-distance links between randomly selected lattice sites. Here, ϕ denotes a prescribed probability for a long-range link to form. In order to minimize finite-size effects, we set the lattice size in each dimension to be $L = 1000$, and employ periodic boundary conditions; i.e., close the square lattice to a two-dimensional torus.

Each of the L^2 lattice sites may be occupied by at most a single individual, represented as a 'particle' with distinct species label S, E, I, A, or R. Once the N individuals have been distributed over the small-world network with a fixed initial density $N/L^2 = 0.1$ of S and I species combined (we start out with zero individuals in either of the states E, A, or R), the simulation proceeds with random sequential updates: A randomly selected individual is allowed to move around and/or react, subject to the set of possible particle reactions prescribed by our modified SEIR model. The control parameters that regulate the speed of the unmitigated infection spread are: the initial densities of particles in each state, the values of the reaction rates depicted in Fig. 1a, and the average connectivity of the small-world network $\langle k \rangle = 4\,(1+\phi)$. On the lattice, upon encounter of a susceptible with an infectious individual, we take the reaction probability for the binary reaction $S + I \to E + I$ to unity. This choices essentially defines the intrinsic simulation time scale.

To model the COVID-19 epidemic on the small-world network, we set the incubation rate to $b = 1/6$ days and the recovery reaction rate as $a = 1/6.5$ days, where $1/b$ and $1/a$ represent the mean incubation and recovery periods, respectively, as reported for this epidemic [19, 16, 20, 21]. The other system parameters are chosen such that the population will suffer epidemic outbreaks, i.e., the system is set above the epidemic threshold, with an effective basic reproduction number tuned to $\mathcal{R}_0 \approx 2.5$, again informed by estimates for COVID-19 [16, 22, 23, 24, 25]. This entails selecting the probability for the formation of long-range links to $\phi = 0.6$, and the population density to 10% of the total number L^2 of lattice sites (here, $N = 10,000$).

2.2 Mitigation strategy

For the current epidemic, delays occur due to the the period before receiving test results, as well as the (unavoidable) time lapse between the identification of infectious individuals and their placement in isolation, and the subsequent time until all infectious persons' contacts are quarantined. As is illustrated in Fig. 2, there are several parameters that can be varied in this scenario: the testing period (TP); the delay between administering the test and isolation of the infected identified individual (DT); the additional delay between isolating positively tested individuals and quarantining their direct contacts (DQ); and the duration of the quarantine (Q).

In the present study, we thus consider the following mitigation protocol:

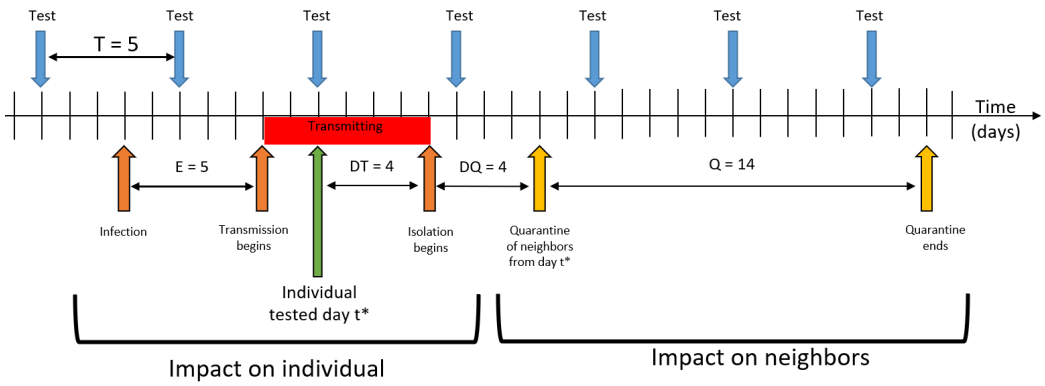

Figure 2: Schematic for the proposed mitigation strategy. Vertical arrows indicate various external actions on the population. The frequency of these control measures and the time delays between the different interventions represent the crucial control parameters for containing the infection.

To be able to capture identified infectious individuals, the population needs to be regularly tested with some prescribed period TP. Testing in the community begins at day ten of the simulation. At some time instant t^*, the entire population, irrespective of the state each individual happens to be in at the time, is considered screened (i.e. full information in the model). Only the identified infectious individuals, however, are registered. These individuals are placed in isolation after some fixed delay time DT. Contact tracing is implemented in our model through registering the information about each identified individual's neighbors along any of the links in the small-world network, at the time t^* of the testing. At the later time t^* + DT + DQ, these nearest neighbors will be placed in quarantine. Subsequently, both the originally identified infectious individuals and their nearest neighbors will be released from quarantine after Q days from the moment they have been isolated. Note that these individuals may change their state from E to I/A and A or I to R with the corresponding fixed rates while in quarantine or isolation. For example, infectious individuals in isolation recover with rate a.

In order to clearly demonstrate the efficacy of this mitigation strategy, it is necessary to set the initial conditions of our dynamical model to admit sizeable outbreaks to occur. To this end, we take the initial number of the infection centers in the system to be $I_0 = 10$, and we start to test and isolate

the individuals 10 days after these infection nuclei were planted in the population. Furthermore, we set the basic model parameters that describe the testing protocol to certain realistic default values, also listed in Table 1; namely IID= 50%: one half of the infectious population is identifiable through the testing, a ratio that incorporates both test availability and reliability; TP = 7 days: periodic testing campaigns are carried out weekly; DT = 2 days: it takes two days for the tests to be evaluated and to arrange for the infectious individuals to be put into isolation; DQ = 2 days: subsequent contact tracing consumes another two days until the immediate contacts (through either short- or long-range links in the small-world network) are quarantined; and Q = 14 days: isolated and quarantined individuals are kept immobile and disconnected from the remainder of the population for two weeks.

3 Results

Variation of the model parameters {TP, DT, DQ, Q} decisively impact the dynamics of the disease spread and the final outcome. We systematically vary our base model parameters within reasonable bounds to probe their impact on the infection outbreak and its potential mitigation.

The simulation data shown in Fig. 3 illustrate the crucial dependence of the infection peak and overall spread in the population on the fraction of identified infectious individuals IID ranging from 10% to 95%. Increasing IID either by means of a larger testing inventory and/or a higher standard of test efficacy naturally reduces the infection peak and overall fraction of infected individuals. For inefficient testing procedures with IID $< 25\%$, the infection curves deviate only weakly from the uncontrolled outbreak. The sensitivity for both infected population peak height and cumulative number

Parameter	Description	Standard Value	Range
IID	identified infectious fraction	50%	10 – 95 %
TP	testing period	7 days	1, 2, 5, 7, 10 days
DT	delay to testing	2 days	1, 2, 5 days
DQ	delay to quarantine	2 days	1, 2 days
Q	quarantine length	14 days	7, 14 days

Table 1: Control parameters varied during mitigation. Figure 2 provides an example of how these variables function and affect the intervention scheme.

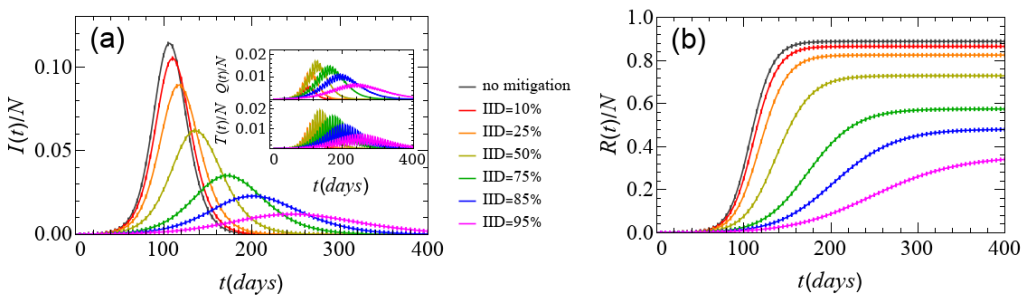

Figure 3: Infection outbreak and recovered population curves for the stochastic SEIR model with mitigation through periodic testing, isolation, and quarantine. (a) Fractions $I(t)/N$ of the infected and (b) $R(t)/N$ of the recovered population as a function of time, plotted for varying percentages of identified infectious individuals (IID = 10% . . . 95%). The unmitigated outbreak curve (black) is shown for reference. The inset in (a) additionally displays the fractions $T(t)/N$ of infectious individuals in **isolation**, and $Q(t)/N$ of individuals in **quarantine** at time t. Note that owing to the smaller population fraction in isolation or quarantine, the periodic variations induced by the testing as well as stochastic fluctuations appear more prominently in these graphs. In all mitigated curves, the testing period (TP = 7 days), delay between test and isolation (DT = 2 days), quarantine duration of nearest neighbors (Q = 14 days), and delay between isolating positively tested individuals and quarantining their direct contacts (DQ = 2 days) are held constant. The data for each curve were averaged over 100 independent realizations; statistical error bars presented here are a similar size to that of the data points.

of recovered individuals is observed to be highest when IID is varied from 25 to 75%. Yet it should be noted that even at IID= 95%, more than 1/3 of the population ultimately falls victim to the disease. The inset in Fig. 3(a) also depicts the fractions of isolated as well as quarantined individuals during the course of the epidemic; these reach sizeable values for IID$\geq$ 25%.

Next we examine the efficacy of the testing control protocol as function of the testing period TP, are shown in Fig. 4. Reducing the testing period systematically and substantially diminishes the infection peak as well as the cumulative number of recovered individuals during the outbreak. However, even daily testing (our lower bound on TP in this study) is not sufficient to fully suppress the outbreak when IID = 50%. In fact, under these conditions, it still leads to more than half the population becoming infected.

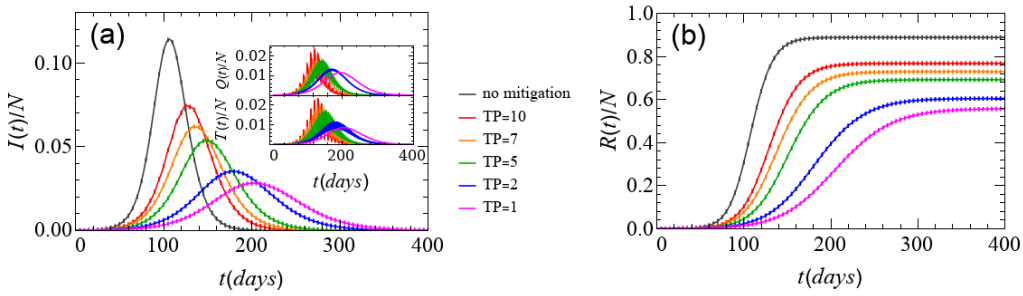

Figure 4: Infection outbreak and recovered population curves for the stochastic SEIR model with periodic testing intervention. (a) Fraction $I(t)/N$ of infected and (b) fraction $R(t)/N$ of the recovered population for different implemented testing periods (TP ranging from 1 to 10 days). The black curve depicts the unmitigated outbreak. The inset in (a) additionally displays the fractions $T(t)/N$ and $Q(t)/N$ of infectious individuals in isolation, and of individuals in quarantine. In all mitigated curves, the percentage of identified infectious individuals (IID = 50%), delay between test and isolation (DT = 2 days), quarantine duration of nearest neighbors (Q = 14 days), and delay between isolating positively tested individuals and quarantining their direct contacts (DQ = 2 days) are kept constant. The data for each curve were averaged over 100 independent realizations; statistical error bars presented here are a similar size to that of the data points.

Inevitable delays in isolating infectious individuals after positive test results are observed, and subsequently in quarantining their direct contacts. These lags may also adversely affect mitigation success. Indeed, as evidenced in Fig. 5, increasing delays in the isolation of positive test cases induce higher peaks in the infection curves and concomitant increases in the cumulative infected population counts. As Fig. 6a illustrates, however, reducing the quarantine period to just one week does increase the infection peak and the total number of recovered individuals, but only by comparatively small amounts. Similarly, an increase in the delay between isolation of positive test cases and the quarantine of their direct contacts, explored in Fig. 6b, causes slightly enhanced infection curve peaks and a minor increase of the cumulative infected population.

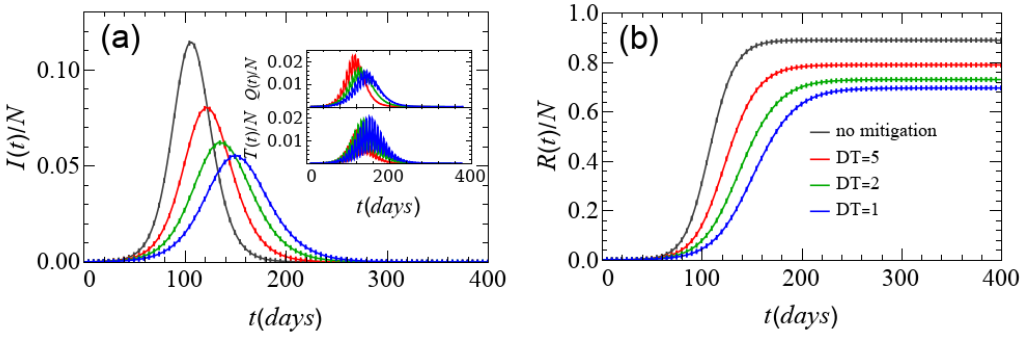

Figure 5: Infection outbreak and recovered population curves for the stochastic SEIR model with various delays in testing. (a) Fraction $I(t)/N$ of infected and (b) fraction $R(t)/N$ of the recovered population for the stochastic SEIR model for different delay times (DT = 1, 2, or 5 days) between test and isolation (unmitigated outbreak curve in black). The inset in (a) additionally displays the fractions $T(t)/N$ of isolated individuals and $Q(t)/N$ of quarantined individuals. In all mitigated curves, the percentage of identified infectious individuals (IID = 50%), testing period (TP = 7 days), quarantine duration of nearest neighbors (Q = 14 days), and delay between isolating positively tested individuals and quarantining their direct contacts (DQ = 2 days) are kept constant. The data for each curve were averaged over 100 independent realizations; statistical error bars presented here are a similar size to that of the data points.

4 Discussion

We summarize our quantitative parameter study data in three heat map plots, Figs. 7a-7c. These graphical representations indicate that for low values of IID and high values of TP, the outbreak remains essentially unmitigated and the infection peak arrives within the first 100 days. In contrast, for an extremely efficient containment of the outbreak, corresponding to a high fraction of IID ($> 70\%$) and frequent (daily) testing, the infection is seen to peak already in the first 50 days of the outbreak, with a considerably lower peak magnitude and drastically reduced total fraction of ever infected individuals as compared with the unmitigated scenario, both indicating that the outbreak is most effectively suppressed.

We note that, e.g., recent work by Kretzschmar et al. demonstrated that a combination of non-pharmaceutical interventions, i.e., both physical dis-

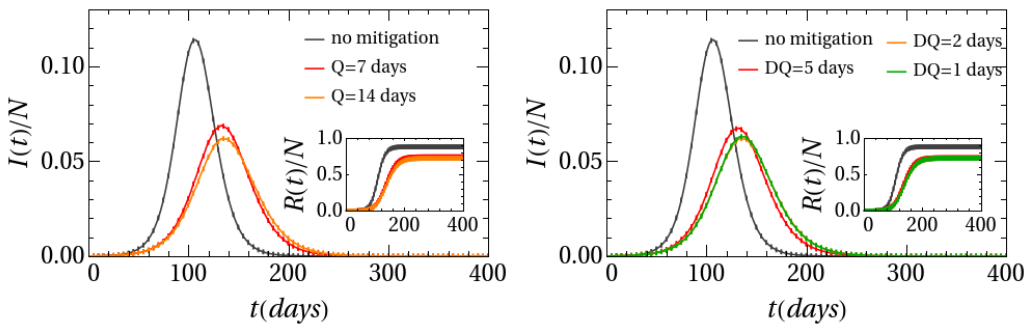

a) b)

Figure 6: Infection outbreak and recovered population curves for the stochastic SEIR model with periodic testing intervention. (a) Fraction $I(t)/N$ of the infected populations, with varying quarantine duration (Q = 7 or 14 days). Here, the delay between isolating positively tested individuals and quarantining their direct contacts (DQ = 2 days) is kept constant. The inset in (a) displays the fraction $R(t)/N$ of recovered individuals. (b) Fraction $I(t)/N$ of the infected populations, with the delay between isolating positively tested individuals and quarantining their direct contacts (DQ = 1, 2, or 5 days). Here, the quarantine duration for nearest neighbors (Q = 14 days) is kept constant. The inset in (b) shows the fraction $R(t)/N$ of recovered individuals. In all mitigated curves, the percentage of identified infectious individuals (IID = 50%), testing period (TP = 7 days), and delay between test and isolation (DT = 2 days) are held constant. The data for each curve were averaged over 100 independent realizations; statistical error bars presented here are a similar size to that the data points.

tancing and contact tracing can reduce the effective reproduction number below the epidemic threshold [26]. Varying the testing and tracing coverage as well as testing and tracing delays, the authors showed that testing delays can significantly increase the potential for onward transmission. With no delay in testing, nearly 80% of transmission is averted while only 5% is averted with a five day delay. They conclude that an advanced contact tracing method via mobile app, which eliminates testing and tracing time delays, is sufficient to quell the infection spread when the testing coverage exceeds 60%. Indeed, it has been claimed that more restrictive, widespread control measures can be substantially alleviated if testing and contact tracing pro-

grams are implemented effectively [27]. Similar to our finding, Grantz et al. determined that test effectiveness constitutes a crucial parameter for containing infectious spreading. According to their simulation results, at least 60% of the infectious population must be captured with testing (assuming perfect quarantine) for spread of the infection to be brought below the epidemic threshold. With more than 50% of infectious individuals identified, we observe significant reductions in the peak of infections and the total number that becomes infected during the epidemic (Figure 3). In contrast, our results require a much larger fraction of infectious individuals to be identified before falling below the epidemic threshold.

Our work assumes perfect adherence to quarantine, i.e., all neighbors of identified infectious individuals are unable to interact with others for the defined quarantine period. Importantly, even for perfect adherence to quarantine not all transmission is averted as some will occur prior to quarantine and isolation. Similar results were reported by Quilty et al., who determined the amount of transmission potential during quarantine or isolation, i.e., the integral of the infectivity curve over time spent in quarantine and post-quarantine isolation, weighted by compliance [28]. They extensively explored the effects of quarantine adherence and suggested that with lower adherence to quarantine, as has been reported in the UK, only a small fraction of potential transmission is averted [29] . Both our work and that of Quilty et al. [28] note that quarantine periods of ten days rather than fourteen may be nearly as effective at averting transmission assuming high compliance.

All three studies, Refs. [26, 28, 27], utilize variations of the well-known branching process for stochastic modeling of the COVID-19 spread. However, since these branching processes were not implemented in a spatial or network setting, these results do not account for potentially decisive spatial correlations that emerge in realistic disease spreading. It is therefore natural and relevant to ask next whether the infectious disease dynamics becomes qualitatively altered if considered in spatially extended models. In previous work, we explored that question by performing individual-based numerical simulations of stochastic Susceptible-Infectious-Recovered (SIR) model variants on four distinct spatially organized lattice and network architectures [9]. We found that highly connected networks closely follow mean-field SIR rate equations, while the disease spread on a lattice and small-world network revealed marked correlation effects. A distinct investigation confirms that the dynamical behavior of infection spreading on networks with the same connectivity distribution could still differ, depending on the net-

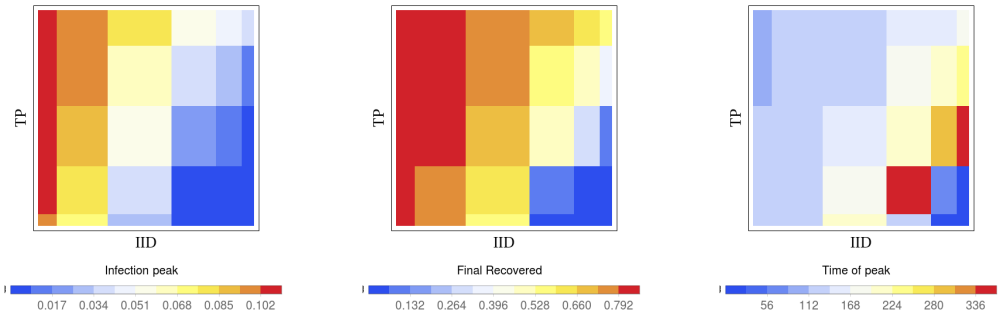

a) b) c)

Figure 7: Heat map representation of pertinent outcomes: The heat map colors in figures (a), (b), and (c) respectively represent the peak in the curve of the fraction of infected individuals, the fraction of the total number of recovered individuals at the end of the outbreak, and the time (in days) at which the infection peaks in the population. The fraction of identified infectious individuals (IID) is varied along the horizontal axis and the testing period (TP in days) is varied along the vertical axis. IID takes values from the set {0.1,0.25,0.5,0.75,0.85,0.95}; TP takes values from the set {1,2,5,7,10} in units of days. In all mitigated curves, the delay between test and isolation (DT = 2 days), quarantine duration of nearest neighbors (Q = 14 days), and delay between isolating positively tested individuals and quarantining their direct contacts (DQ = 2 days) are held constant.

works' subtle construction details such as degree of clustering [30]. Following their results for numerical simulations of stochastic Susceptible-Infectious-Recovered-Susceptible (SIRS) model on a networks with exponential connectivity distribution, some quantities such as the mean number of infected individuals at stochastic equilibrium change with the fine details of the network structure, while others like the basic reproduction ratio R_0 appear to be completely determined by the network's mean connectivity and the connectivity distribution.

5 Conclusion

From our individual-based numerical simulations of infectious disease spreading on a realistically motivated small-world network architecture under par-

tial control through testing and isolation schemes and quarantine of nearest neighbors, we draw the conclusion that a targeted improvement of mitigation protocols through systematic reduction of the testing period and maximization of the fraction of identified infectious individuals constitutes the most effective way of mitigating epidemic outbreaks. In this context we note that deficiencies in test reliability and accuracy can at least partially be compensated by increased testing frequency. Delays in effecting isolation, quarantine, and shortening the quarantine period itself, provided the latter still exceeds the incubation time for the disease, are not as sensitive in reducing the infection peak and the cumulative number of infected individuals in the population; these variables should hence be considered with lower priority for efforts in optimizing testing mitigation protocols.

Acknowledgment

Research was sponsored by the U.S. Army Research Office and was accomplished under Grant Number W911NF-17-1-0156. The views and conclusions contained in this document are those of the authors and should not be interpreted as representing the official policies, either expressed or implied, of the Army Research Office or the U.S. Government. The U.S. Government is authorized to reproduce and distribute reprints for Government purposes notwithstanding any copyright notation herein. L.M.C. acknowledges support of NSF RAPID Grant Number 2029262. S.S. acknowledges support from the Fralin Biomedical Research Institute. S.D. acknowledges a fellowship from the China Scholarship Council (CSC) under Grant CSC Number 201806770029.

References

[1] Kermack WO, McKendrick AG. 1927. A contribution to the mathematical theory of epidemics. Proc R Soc Lond A **115**, 700–721. (http://dx.doi.org/10.1098/rspa.1927.0118 doi:10.1098/rspa.1927.0118).

[2] Brauer F. 2017. Mathematical epidemiology: Past, present, and future. Infect Dis Model **2**, 113–

127. (http://dx.doi.org/10.1016/j.idm.2017.02.001 doi:10.1016/j.idm.2017.02.001).

[3] Anderson RM, May RM 1992. Infectious diseases of humans: dynamics and control. Oxford university press.

[4] Keeling MJ, Rohani P 2011. Modeling infectious diseases in humans and animals. Princeton University Press.

[5] Murray JD 2002. Mathematical Biology, Vols. I + II. Springer, New York, 3rd ed.

[6] Täuber UC 2014. Critical Dynamics – A Field Theory Approach to Equilibrium and Non-Equilibrium Scaling Behavior. Cambridge University Press, Cambridge.

[7] Lindenberg K, Metzler R, Oshanin G, (Eds.) 2019. Chemical Kinetics: Beyond the Textbook. World Scientific, London.

[8] Eubank S, Eckstrand I, Lewis B, Venkatramanan S, Marathe M, Barrett CL. 2020. Commentary on Ferguson, *et. al* Impact of Non-pharmaceutical Interventions (NPIs) to Reduce COVID-19 Mortality and Healthcare Demand **82**, 52–59. (http://dx.doi.org/10.1007/s11538-020-00726-x doi:10.1007/s11538-020-00726-x).

[9] Mukhamadiarov RI, Deng S, Serrao SR, Priyanka, Nandi R, Yao LH, et al. 2020. Social distancing and epidemic resurgence in agent-based Susceptible-Infectious-Recovered models. (http://arxiv.org/abs/2006.02552 arXiv:2006.02552).

[10] Salathé M, Kazandjieva M, Lee JW, Levis P, Feldman MW, Jones JH. 2010. A high-resolution human contact network for infectious disease transmission. Proceedings of the National Academy of Sciences **107**, 22020–22025. (http://dx.doi.org/10.1073/pnas.1009094108 doi:10.1073/pnas.1009094108).

[11] Eames K, Bansal S, Frost S, Riley S. 2015. Six challenges in measuring contact networks for use in modelling. Epidemics **10**, 72–77. (http://dx.doi.org/10.1016/j.epidem.2014.08.006 doi:10.1016/j.epidem.2014.08.006).

[12] Nishiura H, Kobayashi T, Miyama T, Suzuki A, Jung Sm, Hayashi K, et al. 2020. Estimation of the asymptomatic ratio of novel coronavirus infections (COVID-19). International Journal of Infectious Diseases **94**, 154–155. (http://dx.doi.org/10.1016/j.ijid.2020.03.020 doi:10.1016/j.ijid.2020.03.020).

[13] Tindale LC, Stockdale JE, Coombe M, Garlock ES, Lau WYV, Saraswat M, et al. 2020. Evidence for transmission of COVID-19 prior to symptom onset. elife **9**, e57149. (http://dx.doi.org/10.7554/eLife.57149 doi:10.7554/eLife.57149).

[14] Kraemer MUG, et al. 2020. The effect of human mobility and control measures on the COVID-19 epidemic in China. Science **368**, 493–497. (http://dx.doi.org/10.1126/science.abb4218 doi:10.1126/science.abb4218).

[15] Fu H, Xi X, Haowei H Wang, et al. 2020. The COVID-19 epidemic trends and control measures in mainland China. Imperial College London. (http://dx.doi.org/10.25561/80360 doi:10.25561/80360).

[16] Ferguson NM, et al. 2020. Impact of non-pharmaceutical interventions (NPIs) to reduce COVID-19 mortality and healthcare demand. Imperial College London. (http://dx.doi.org/10.25561/77482 doi:10.25561/77482).

[17] Delamater PL, Street EJ, Leslie TF, Yang Y, Jacobsen KH. 2019. Complexity of the Basic Reproduction Number (R0) **25**, 1–4. (http://dx.doi.org/10.3201/eid2501.171901 doi:10.3201/eid2501.171901).

[18] Newman MEJ, Watts DJ. 1999. Scaling and percolation in the small-world network model. Phys Rev E **60**, 7332–7342. (http://dx.doi.org/10.1103/PhysRevE.60.7332 doi:10.1103/PhysRevE.60.7332).

[19] Qin J, You C, Lin Q, Hu T, Yu S, Zhou XH. 2020. Estimation of incubation period distribution of COVID-19 using disease onset forward time: A novel cross-sectional and forward follow-up study. Sci Adv **6**, 1–7. (http://dx.doi.org/10.1126/sciadv.abc1202 doi:10.1126/sciadv.abc1202).

[20] He X, Lau EH, Wu P, Deng X, Wang J, Hao X, et al. 2020. Temporal dynamics in viral shedding and transmissibility of COVID-19. Nature Medicine **26**, 672–675. (http://dx.doi.org/10.1038/s41591-020-0869-5 doi:10.1038/s41591-020-0869-5).

[21] McAloon C, Collins Á, Hunt K, Barber A, Byrne AW, Butler F, et al. 2020. Incubation period of COVID-19: a rapid systematic review and meta-analysis of observational research. BMJ Open **10**, e039652. (http://dx.doi.org/10.1136/bmjopen-2020-039652 doi:10.1136/bmjopen-2020-039652).

[22] Li R, Pei S, Chen B, Song Y, Zhang T, Yang W, et al. 2020. Substantial undocumented infection facilitates the rapid dissemination of novel coronavirus (SARS-CoV-2). Science **368**, 489–493. (http://dx.doi.org/10.1126/science.abb3221 doi:10.1126/science.abb3221).

[23] Petersen E, Koopmans M, Go U, Hamer DH, Petrosillo N, Castelli F, et al. 2020. Comparing SARS-CoV-2 with SARS-CoV and influenza pandemics. The Lancet Infectious Diseases **20**, e238– e244. (http://dx.doi.org/10.1016/S1473-3099(20)30484-9 doi:10.1016/S1473-3099(20)30484-9).

[24] Salje H, Kiem CT, Lefrancq N, Courtejoie N, Bosetti P, Paireau J, et al. 2020. Estimating the burden of SARS-CoV-2 in France. Science **369**, 208–211. (http://dx.doi.org/10.1126/science.abc3517 doi:10.1126/science.abc3517).

[25] Li Q, Guan X, Wu P, Wang X, Zhou L, Tong Y, et al. 2020. Early transmission dynamics in Wuhan, China, of novel coronavirus–infected pneumonia. New England Journal of Medicine **382**, 1199–1207. (http://dx.doi.org/10.1056/NEJMoa2001316 doi:10.1056/NEJMoa2001316).

[26] Kretzschmar ME, Rozhnova G, Bootsma MC, van Boven M, van de Wijgert JH, Bonten MJ. 2020. Impact of delays on effectiveness of contact tracing strategies for COVID-19: a modelling study. The Lancet Public Health **5**, e452–e459. (http://dx.doi.org/10.1016/S2468-2667(20)30157-2 doi:10.1016/S2468-2667(20)30157-2).

[27] Grantz KH, Lee EC, McGowan LD, Lee KH, Metcalf CJE, Gurley ES, et al. 2020. Maximizing and evaluating the impact of test-trace-isolate programs. medRxiv. (http://dx.doi.org/10.1101/2020.09.02.20186916 doi:10.1101/2020.09.02.20186916).

[28] Quilty BJ, Clifford S, Flasche S, Kucharski AJ, Edmunds WJ, Group CCW, et al. 2020. Quarantine and testing strategies in contact tracing for SARS-CoV-2. medRxiv. (http://dx.doi.org/10.1101/2020.08.21.20177808 doi:10.1101/2020.08.21.20177808).

[29] Smith LE, Potts HW, Amlot R, Fear NT, Michie S, Rubin J. 2020. Adherence to the test, trace and isolate system: results from a time series of 21 nationally representative surveys in the UK (the COVID-19 Rapid Survey of Adherence to Interventions and Responses [CORSAIR] study). medRxiv. (http://dx.doi.org/10.1101/2020.09.15.20191957 doi:10.1101/2020.09.15.20191957).

[30] Ames GM, George DB, Hampson CP, Kanarek AR, McBee CD, Lockwood DR, et al. 2011. Using network properties to predict disease dynamics on human contact networks. Proc R Soc B **278**, 3544–3550. (http://dx.doi.org/10.1098/rspb.2011.0290 doi:10.1098/rspb.2011.0290).